

# Viscoelastic effects in nanometer-scale contacts under shear

K.J. Wahl, S.V. Stepnowski<sup>a)</sup>, and W.N. Unertl<sup>b)</sup>

Code 6170, Naval Research Laboratory, Washington, D.C. 20375-5342

<sup>a)</sup>USNR, The George Washington University NROTC Unit, Washington DC 20052.

<sup>b)</sup>On sabbatical leave from Department of Physics and Astronomy, University of Maine, Orono, ME 04469-5764.

We demonstrate the effects of shear modulation on the viscoelastic response of nanometer-scale single-asperity contacts under static and dynamic loading conditions. Contact stiffness and relaxation time are determined for contacts to poly(vinylethylene) using a scanning force microscope (SFM). Knowledge of the torsional stiffness  $k_Q$  of the SFM cantilever is not required to determine the relaxation time. The relaxation time was several orders of magnitude slower than the bulk relaxation time but decreased slowly to the bulk value as the sample age increased. Contacts showed no evidence of microslip. We show that the shear response observed during the making and breaking of the contacts provides information about the time evolution of the contact area that is not available in force vs. distance curve measurements.

**Keywords:** Nano-tribology, viscoelastic contacts, shear modulation, scanned force microscope, poly(vinylethylene), single asperity contacts

## 1. Introduction

Nanometer-scale single asperity contacts have broad importance in tribology. They are a key element in microscopic models of macroscopic contacts as formulated by Bowden and Tabor [1], their sizes are comparable to mechanical contacts in MEMS devices [2], and they are widely used as models of AFM contacts [3]. In each of these areas, it is essential to understand the mechanical behavior of the contact, particularly under combined normal and shear loading. In this letter we describe new experiments using the scanning force microscope (SFM) to demonstrate the effects of viscoelasticity on the mechanical properties of single asperity contacts. The possibility of making these measurements was suggested previously [4]. The method is based on well-developed mechanical modulation techniques used to measure the viscoelastic mechanical properties of bulk polymers [5] and has been used previously to study elastic behavior in SFM contacts [6-8]. Similar methods have also been applied to much larger diameter contacts using the surface forces apparatus [9,10] and microscopic sphere-on-flat contacts [11]. The technique is also closely related to friction loop methods [12] and to SFM methods that use modulation normal to the sample surface [13,14].

Figure 1a illustrates schematically how the shear response is measured. An SFM tip of height  $H$ , mounted on a cantilever force sensor, is initially in contact with a viscoelastic sample above  $O$  under applied load  $F_N$ . The substrate is displaced parallel to its surface by distance  $x_o$  to  $O'$ . This causes a displacement of the center of the contact by  $x_t = x_o - x_c$  where  $x_c$  is the distortion of the sample surface relative to point  $O'$ . This distortion results from the shear force  $F_s = k_Q x_t$ , where  $k_Q$  is the torsional stiffness of the cantilever. For a viscoelastic material and oscillatory

sample displacement  $x_o(t) = X_o \exp(i\omega t)$ , there is a phase lag in the response of the contact so that  $x_c = X_c \exp[i(\omega t + \beta)]$  and  $x_t = X_t \exp[i(\omega t - \alpha)]$ . (See the phasor diagram, Fig. 1b). The experimentally measured quantities are the amplitude and phase of the tilt angle  $Q$  of the tip,  $Q = x_t / H = Q_o \exp[i(\omega t - \alpha)]$  where  $Q_o \equiv X_t / H$ . The shear stiffness of the contact is  $k_\xi \equiv dF_s / dx_c$ .

The relaxation time  $\tau$  of the polymer surface associated with its viscoelastic response is of interest because it can be related to the effects of intermolecular constraints on segmental relaxation [15,16]. We estimate  $\tau$  using the simple mechanical Voigt model [17]. In this model, the viscoelastic component of the contact is described by a linear spring of stiffness  $k_\xi$  in parallel with a dashpot with damping coefficient  $r_c$ . The cantilever is modeled by a linear spring of stiffness  $k_Q$  in series with the Voigt model. The stiffness  $k_\xi$  is related to the effective storage shear modulus  $G^*$  [5]. For the case of an elastic Hertzian contact with no slip,  $k_\xi = 8G^*a$  where  $a$  is the effective radius of the contact [8,18]. This mechanical model is described by the differential equation  $F = k_\xi x_c + r_c dx_c / dt = k_Q x_t$  where  $x_c$  and  $x_t$  are as defined above. Force,  $F = F_o \exp[i(\omega t - \mathbf{g})]$ , is related to the quantities  $X_t$  and  $\mathbf{a}$  by  $F_o = k_Q X_t$  and  $\mathbf{a} = \mathbf{g}$ . The stiffness of the contact is given in terms of the measurable quantities shown in Fig. 1 by

$$k_\xi = k_Q \frac{\left(\frac{X_t}{X_o}\right) \cos \mathbf{a} - \left(\frac{X_t}{X_o}\right)^2}{1 + \left(\frac{X_t}{X_o}\right)^2 - 2\left(\frac{X_t}{X_o}\right) \cos \mathbf{a}} \quad (1)$$

and the response time  $t$  by

$$t = \frac{r_c}{k_\zeta} = \frac{\tan(b-a)}{2pf} \quad (2)$$

where

$$\sin b = \left[ \frac{(X_t/X_o)}{\sqrt{1+(X_t/X_o)^2 - 2(X_t/X_o)_t \cos a}} \right] \sin a$$

and  $f$  is frequency.  $t$ , as determined from eqn.(2), is a particularly robust quantity since it depends only on the measured phase  $\alpha$  and the ratio of measured amplitudes  $X_t/X_o$ , and does not require knowledge of the cantilever torsional stiffness  $k_\zeta$ .

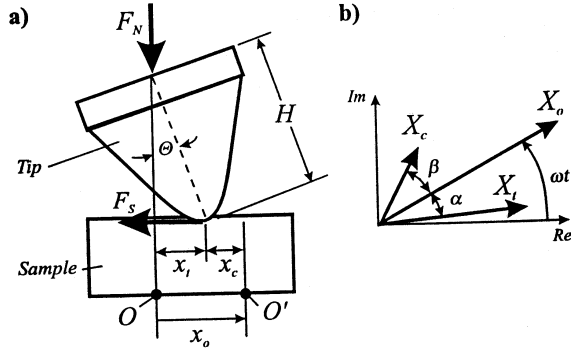


FIG 1. (a) Schematic diagram of the SFM shear measurement. (b) Phasor diagram relating the amplitudes and phases of the drive signal  $X_o$ , tip motion  $X_t$ , and contact motion  $X_c$ .

## 2. Experimental

The SFM we used has been described previously [19] and is based on the optical lever method. The sample was oscillated laterally with respect to the cantilever by applying a small sinusoidal modulation to the piezoelectric scan tube, and the response of the scan tube was determined using the double piezoelectric response method of Chen [20]. Torsional response of the SFM cantilever was obtained from the photodiode output with a lock-in amplifier. This signal can be converted into a shear force acting on the tip if the torsional force constant  $k_\zeta$ , and tip height,  $H$

are known. For the cantilevers we used [21],  $k_\zeta \approx (66.6 \text{ N/m})$  [22], and  $H \approx 4 \mu\text{m}$  as determined with a scanning electron microscope. We use these values in calculations.  $X_o$  was calibrated using measurements on diamond, whose shear modulus is about  $10^5$  times larger than poly(vinylethylene), PVE. This avoids the need to directly measure the lateral response of the scan tube for driving

amplitudes smaller than 20 mV (about 0.5 nm actual deflection). Possible deformation of the tip [7] was ignored.

The un-cross-linked PVE samples were made from the same 96% 1,2-polybutadiene material with 134,000 number-average molecular weight used in a previous study of the bulk mechanical properties [15,16]. From this study, the measured relaxation time at 295 K is  $t_d \approx 60 \mu\text{s}$ . Young's modulus was measured by indentation to be in the range 2-4 MPa. Films of un-cross-linked PVE were cast onto glass slides from toluene solution, dried in air for about 10-15 min, followed by vacuum drying for another 10-20 min.

## 3. Results and Discussion

Figure 2 compares typical shear response data for freshly cleaved mica and PVE with an applied load of about 2 nN. For mica, which is an elastic material, the response amplitude  $X_t$  increased linearly (Fig. 2a) and  $\alpha$  was constant and equal to  $0^\circ$  (Fig. 2b) until a maximum drive amplitude  $X_o^{max} \approx 40 \text{ mV}$  ( $\approx 2 \text{ nm}$ ). At this point,  $X_t$  suddenly decreased and  $\alpha$  increased. This is the behavior expected when the contact begins to slide [9,23,24]. In the case of the much softer PVE,  $X_t$  also increased linearly up to 125 mV, (the largest value studied) but with a smaller slope and a phase lag  $\alpha = 42^\circ$ . The shear response (i.e., the slope in Fig. 2a) of PVE was measured from 50 Hz to 1.2 kHz and the phase lag  $\alpha$  (■'s in Fig. 2c) varied with frequency  $f$ . This frequency dependent phase change is direct evidence that the contact is viscoelastic [5].

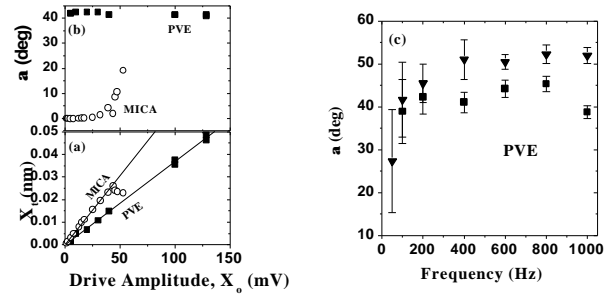


FIG. 2. Shear response (a) amplitude  $X_t$  and (b) phase  $a$  as a function of drive amplitude  $X_o$  for mica and PVE;  $F_N = 2 \text{ nN}$ . (c) Frequency dependence of phase lag  $\alpha$  for PVE measured at constant load (■'s) and at maximum load during a force-distance curve measurement (▼'s) such as that shown in Fig. 3.

The linear behavior of mica and PVE in Fig. 2a is somewhat surprising from the viewpoint of contact mechanics. Micro-slip near the edge of the contact is predicted to reduce  $F_s$  for a given  $x_c$  [8,18,25] and this behavior has been verified for macroscopic contacts [26]. Peeling may also be possible at small displacements and would also produce a nonlinear response [25,27]. Linear response is only expected in the limit of small shear displacements or in the

idealized case of a Hertzian contact with static friction; i.e., no slip anywhere inside the contact [25]. In this case,  $F_s = (8G^*a)x_c$ . The linear behavior shown in Fig. 2a indicates that studies of small contacts under shear should prove valuable for testing the limits of continuum contact mechanics. The contact radius for  $F_N$  can be estimated from a Sneddon analysis of the contact and shows that the contact radius is approximately equal to the nominal tip radius.

PVE is so compliant that, even for the small forces used here, the usual approximation that the diameter of the contact is much smaller than the probe is not satisfied. Appropriate expressions for an elastic indentation by a spherical punch are given by Sneddon [28] and Maugis [29]. We know of no treatment for the case of shear. The contact radius for  $F_N$  can be estimated from a Sneddon analysis of the contact and shows that the contact radius is approximately equal to the nominal tip radius.

Another way to measure the viscoelastic shear response is to apply the shear during a force-distance curve measurement; i.e., during the formation, loading, unloading, and rupture of a contact [4]. Figure 3 shows data for a freshly prepared PVE substrate obtained at  $f = 1.0$  kHz. The origin for the time axis is taken at the point of maximum applied load (C). The lower panel displays the force-distance curve [30]. The sample was moved toward the tip at constant speed starting out of contact. Jump-to-contact occurred at point A ( $t = -36$  s). The approach continued until a predetermined maximum load at C ( $t = 0$  s). Then the direction of motion was reversed until the tip and sample separated at the pull-off point E ( $t = 164$  s). The rounding just prior to pull-off is typical of both macroscopic and SFM-scale viscoelastic contacts [31,32]; the magnitude of the pull-off force and the degree of rounding depend on the speed, again indicative of the viscoelastic nature of the contact. For times between points B and D, the contact was under compressive load; otherwise, the load was tensile. The force-distance curve was identical with and without shear modulation indicating that the applied shear modulation does not significantly modify the development of the contact.

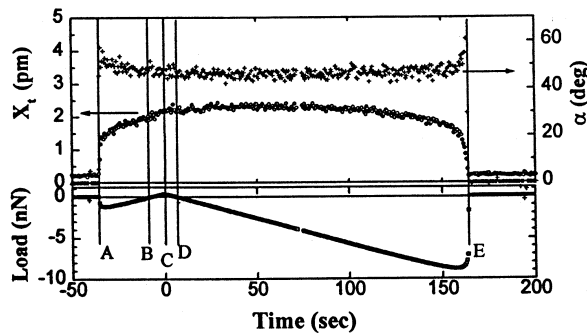


FIG. 3. Shear response of a freshly prepared PVE sample at 1.0 kHz. Lower panel: force-distance curve. Upper panel: amplitude  $X_t$  and phase  $\alpha$  of tip motion on the surface.

The upper panel shows the displacement  $X_t$  and phase  $\alpha$  of the SFM tip. At jump-to-contact (A),  $X_t$  jumped suddenly to about 1.3 pm, then increased more slowly to about 2.4 pm at maximum load (C).  $X_t$  continued to increase slightly until  $t \approx 60$  s even after maximum load was reached, then gradually decreased. This decrease became steeper once the force-distance curve began to round significantly just prior to pull-off (E). Phase response mirrored the amplitude response:  $\alpha$  increased rapidly to about  $60^\circ$ , then decreased slightly, reaching a minimum of about  $43^\circ$  at the same time  $X_t$  reached a maximum. For both amplitude and phase response, the rate of change during jump-to-contact (at A) and pull-off (at E) is limited by the overall response of the measuring system. The large decrease in phase just after A and the increase just prior to E may indicate that sliding occurs just after jump-to-contact as well as just prior to pull-off.

Measurements on PVE were carried out over the range  $50 \text{ Hz} \leq f \leq 1.2 \text{ kHz}$  and were all qualitatively similar to the results for 1.0 kHz (Fig. 3) except that  $X_t$  and  $\alpha$  varied with frequency due to the viscoelastic character of the contact [5]. Results were very reproducible for constant speed and maximum load. The maximum  $X_t$  and corresponding minimum  $\alpha$  always occurred after the contact was under tension, even for the slowest speeds (50 pm/s). This delayed maximum seems to be a characteristic of viscoelastic materials and was not observed for any of the elastic materials we have also studied; e. g., diamond, mica, silicone [33]. For the data in Fig. 3,  $X_t/X_o \ll 1$ , so that eqn. (1) can be written as  $a \cong (kq/8G^*)(X_t/X_o)\cos\alpha$ . Thus, the torsional response of the force sensor is a measure of the contact radius  $a$  as has been pointed out previously for elastic materials [6]. The delayed maximum indicates that  $a$  reaches its maximum value some time after the maximum load has been applied. Ting [34] has predicted this behavior for Hertzian contacts in the absence of adhesion and dispersion forces.

The frequency dependence of  $\alpha$  measured at maximum load (e. g., Fig. 3, point C) is plotted in Fig. 2c ( $\circ$ 's). These values are slightly higher than the values determined from the linear response data ( $\blacksquare$ 's), partly because the

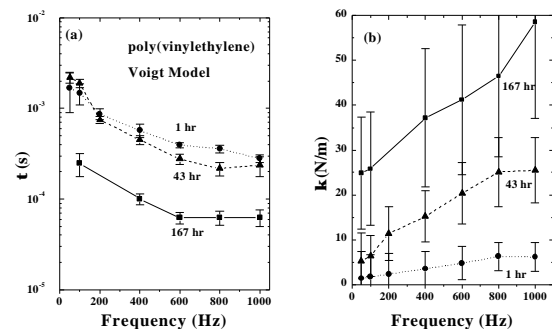


Fig. 4. Voigt model analysis of (a) the response time  $\tau$  and (b) stiffness  $\kappa$  of the contact showing changes as a function of sample age for PVE.

contact area had not reached its steady state value and partly because the measurements were made on a sample that had not aged as long, which we discuss below. Part of the difference may also be due to intrinsic heterogeneities on the PVE surface.

Equations (1) and (2) were used to calculate  $t$  and  $k_c$ . The results are plotted in Fig. 4a and b, respectively, for PVE as a function of sample age, again using data from the maximum load point in Fig. 3. For the as-prepared sample (age  $\leq 1$  hr),  $t$  was about 2 ms at 50 Hz and decreased to about 0.3 ms at 1 kHz (Fig. 4, 's). This reduction in  $t$  was accompanied by an increase in the stiffness  $k_c$  of the contact: i.e., as  $f$  increased, the contact became more glassy, just as observed for the bulk [5]. As the sample age increases,  $t$  approaches the 60  $\mu$ s value observed for bulk PVE [16]. After 167 hr (■'s), the zero frequency stiffness corresponds to  $G^* \approx 2$  MPa and is the same as the bulk value.

#### 4. Summary

In summary, we have demonstrated the effects of viscoelastic response to shear deformation in nanometer-scale contacts. In particular, we show in equation (2) that knowledge of the torsional stiffness  $k_\theta$  of the SFM cantilever is not required to determine the relaxation time  $t$ . As the age of the poly(vinylethylene) sample increased, the contact became more elastic and the effective modulus and relaxation time approached bulk values. As predicted by Ting for Hertzian contacts, the maximum contact area occurred during the loading cycle well after the maximum load is applied. Our experiments also show that shear modulation appears to provide an excellent way study the formation and breaking of small contacts, as well as to test the predictions of contact mechanics theories in the limit of small contacts.

#### Acknowledgements

The authors thank C.M. Roland for providing the PVE samples, R.N. Bolster for measuring Young's modulus, T. Gilbert for diamond sample preparation, as well as R. J. Colton, K. L. Johnson, and R.W. Carpick for useful discussions and encouragement. The authors also thank the Office of Naval Research for support.

#### References

- [1] F. P. Bowden and D. Tabor, *The Friction and Lubrication of Solids* (Clarendon Press, Oxford, 1950).
- [2] R. Maboudian and R.T. Howe, *J. Vac. Sci. Technol. B* **15** (1997) 1.
- [3] N. A. Burnham and R. J. Colton in *Scanning Tunneling Microscopy and Spectroscopy*, ed. D. A. Bonnell (VCH Publishers, Inc., New York, 1993).
- [4] K. Yamanaka and E. Tomita, *Jpn. J. Appl. Phys.* **34** (1995) 2879.
- [5] J. D. Ferry, *Viscoelastic Properties of Polymers* (John Wiley, New York, 1980).
- [6] R. W. Carpick, D. F. Ogletree, and M. Salmeron, *Appl. Phys. Lett.* **70** (1997) 1548.
- [7] M. A. Lantz, S. J. O'Shea, A. C. F. Hoole, and M. E. Welland, *Appl. Phys. Lett.* **70** (1997) 970.
- [8] M. A. Lantz, S. J. O'Shea, M. E. Welland, and K. L. Johnson, *Phys. Rev. B* **55** (1997) 10776.
- [9] G. Luengo, F. J. Schmitt, R. Hill, and J. Israelachvili, *Macromolecules* **30** (1997) 2482.
- [10] S. Granick and H. W. Hu, *Langmuir* **10** (1994) 3857.
- [11] J. M. Georges, A. Tonck, J. L. Loubet, D. Mazuyer, E. Georges, and F. Sidoroff, *J. Phys. II France* **6** (1996) 57.
- [12] S. R. Cohen, G. Neubauer, and G. M. McClelland, *J. Vac. Sci. Technol. A* **8** (1990) 3449.
- [13] N. A. Burnham, G. Gremaud, A. J. Kulik, P. J. Gallo, and F. Oulevey, *J. Vac. Sci. Technol. B* **14** (1996) 1308.
- [14] K. Tanaka, A. Taura, S. R. Ge, A. Takahara, and T. Kajiyama, *Macromolecules* **29** (1996) 3040.
- [15] J. Colmenero, A. Alegria, P. G. Santangelo, K. L. Ngai, and C. M. Roland, *Macromolecules* **27** (1994) 407.
- [16] C. M. Roland, *Macromolecules* **27** (1994) 4242.
- [17] *Shock and Vibration Handbook*, 4<sup>th</sup> edition, ed. C. M. Harris (McGraw-Hill, New York, 1996) p. 2.5.
- [18] K. L. Johnson, *Contact Mechanics* (Cambridge University Press, Cambridge, United Kingdom, 1985).
- [19] D. D. Koleske, G. U Lee, B. I. Gans, K. P. Lee, D. P. DiLella, K. J. Wahl, W. R. Barger, L. J. Whitman, and R. J. Colton, *Rev. Sci. Instrum.* **66** (1995) 4566.
- [20] C. J. Chen, *Introduction to Scanning Tunneling Microscopy* (Oxford University Press, Oxford, 1993), p. 229.
- [21] D microlevers, Park Scientific Instruments, Sunnyvale, CA.
- [22] D. F. Ogletree, R. W. Carpick, and M. Salmeron, *Rev. Sci. Instrum.* **67** (1996) 3298.
- [23] J. Colchero, M. Luna, and A. M. Baró, *Appl. Phys. Lett.* **68** (1996) 2896.
- [24] T. Baumberger in *Physics of Sliding Friction*, editors: B. N. J. Persson and E. Tosatti (Kluwer Academic Publishers, Dordrecht, 1996), p. 1.
- [25] A. R. Savkoor in *Fundamentals of Friction: Macroscopic and Microscopic Processes*, editors I.L. Singer and H.M. Pollock (Kluwer Academic Publishers, 1992), p. 111.
- [26] K. L. Johnson, *Proc. Roy. Soc. Lond A* **230** (1955) 531.
- [27] A. R. Savkoor and G. A. D. Briggs, *Proc. Roy. Soc. Lond. A* **356** (1977) 103.
- [28] J. N. Sneddon, *Int. J. Eng.* **3** (1965) 47.
- [29] D. Maugis, *Langmuir* **11** (1995) 679.
- [30] See e.g. N.A. Burnham, R.J. Colton, and H.M. Pollock, *Nanotechnology* **4** (1993) 64.
- [31] M Barquins, *J. Adhesion* **14** (1982) 63.
- [32] J. P. Aimé, Z. Elkaakour, C. Odin, T. Bouhacina, D. Michel, J. Curély, and A. Dautant, *J. Appl. Phys.* **76** (1994) 754.
- [33] K. J. Wahl, S. V. Stepnowski and W. N. Unertl (to be published).
- [34] T. C. T. Ting, *J. Appl. Mech.* **33** (1966) 845.